Equatorial heat accumulation as a long-term trigger of permanent Antarctic ice sheets during the Cenozoic

Maxime Tremblin, Michaël Hermoso, Fabrice Minoletti

▶ To cite this version:

HAL Id: hal-01376097
https://hal.science/hal-01376097

Submitted on 25 Nov 2016

Equatorial heat accumulation as a long-term trigger of permanent Antarctic ice sheets during the Cenozoic

Maxime Tremblin[a], Michaël Hermoso[b], and Fabrice Minoletti[a,1]

[a]Institut des Sciences de la Terre de Paris (UMR UPMC/CNRS 7193 ISTeP), Université Pierre et Marie Curie, CNRS, Sorbonne Universités, 75252 Paris Cedex 05, France; and [b]Department of Earth Sciences, University of Oxford, Oxford OX1 3AN, United Kingdom

Growth of the first permanent Antarctic ice sheets at the Eocene−Oligocene Transition (EOT), ~33.7 million years ago, indicates a major climate shift within long-term Cenozoic cooling. The driving mechanisms that set the stage for this glaciation event are not well constrained, however, owing to large uncertainties in temperature reconstructions during the Eocene, especially at lower latitudes. To address this deficiency, we used recent developments in coccolith biogeochemistry to reconstruct equatorial Atlantic sea surface temperature (SST) and atmospheric pCO_2 values from pelagic sequences preceding and spanning the EOT. We found significantly more variability in equatorial SSTs than previously reported, with pronounced cooling from the Early to Middle Eocene and subsequent warming during the Late Eocene. Thus, we show that the Antarctic glaciation at the Eocene−Oligocene boundary was preceded by a period of heat accumulation in the low latitudes, likely focused in a progressively contracting South Atlantic gyre, which contributed to cooling high-latitude austral regions. This prominent redistribution of heat corresponds to the emplacement of a strong meridional temperature gradient that typifies icehouse climate conditions. Our equatorial coccolith-derived geochemical record thus highlights an important period of global climatic and oceanic upheaval, which began 4 million years before the EOT and, superimposed on a long-term pCO_2 decline, drove the Earth system toward a glacial tipping point in the Cenozoic.

Eocene−Oligocene climate transition | coccolith-based proxies | Atlantic equatorial SSTs | Cenozoic pCO_2 | meridional temperature gradient

Significance

The long-term cooling trend of the Cenozoic is punctuated by shorter-term climatic events, such as the inception of permanent ice sheets on Antarctica at the Eocene−Oligocene Transition (~33.7 Ma). Taking advantage of the excellent state of preservation of coccolith calcite in equatorial Atlantic deep-sea cores, we unveil progressive tropical warming in the Atlantic Ocean initiated 4 million years prior to Antarctic glaciation. Warming preceding glaciation may appear

counterintuitive, but we argue that this long-term climatic precursor to the EOT reinforced cooling of austral high latitudes via the redistribution of heat at the surface of the oceans. We discuss this new prominent paleoceanographic and climatic feature in the context of over- arching pCO_2 decline and the establishment of an Antarctic circumpolar current.

The warm, greenhouse Eocene Epoch exhibits climatic pat- terns that remain difficult to constrain, in part because of unreliable low-latitude sea surface temperature (SST) reconstructions (1). So far, only a handful of sites serve as a reference for climate history at low latitudes during the Eocene and the Eocene–Oligocene Transition (EOT): the nearshore Tanzania in the Indian Ocean [Tanzania Drilling Project (TDP)] (1, 2) and open ocean sites in the equatorial Atlantic [Ocean Drilling Program sites ODP 925 and 929] (3–5). These records exhibit rather conflicting proxy data for the TDP and overall long-term cooling for the Atlantic sites 925 and 929. There is, however, no clear and significant cooling trend from the Early to Middle Eocene that indicates the termination of the Early Eocene Climatic Optimum (Fig. 1A). Furthermore, recent quality-checked SSTs for ODP 925 and 929 sites using the Ring Index indicate relatively similar temperatures between the Late Eocene and the Early Oligocene (5). In contrast, high-latitude sites are consistent in demonstrating appreciable cooling of austral subpolar regions during much of the Eocene (3, 4, 6–8). This apparent lack of substantial temperature change in the intertropical belt during the Eocene and across the EOT remains an enigmatic feature that complicates our understanding of the interplay between seawater temperatures at a global scale, pCO_2, and changes in global ocean circulations in the context of new Southern Ocean gateways (9–14). The paucity of low-latitude data, especially in the Pacific Ocean, prevents the reconstruction of the latitudinal temperature gradient, much needed for the successful modeling of processes that drove the greenhouse to icehouse transition (10, 15, 16).

As an alternative to the relatively poor preservation of the foraminifera and issues with the calibration of organic-based proxies (1, 5, 17), this study exploits the coccoliths as a source of paleoclimatic information. Coccolithophores, single-celled phytoplankton algae, are a key component of the carbon cycle and the ocean biological pump, and their calcite biominerals, the coccoliths, are a major component of pelagic sediments. Coccoliths are produced in the mixed layer and, as such, are ideally suited to record the chemistry and temperature of ocean surface waters. Their excellent preservation, even in warm and high pCO_2 settings (18), may overcome methodological caveats associated with the absence or frequent recrystallization of foraminiferal shells (1, 2, 17). Recent culture and sedimentary studies have produced new coccolith-based proxies that make it possible to exploit this underexplored paleoclimatic archive (SI Materials and Methods) (19–21). In the present

study, we used the established temperature dependence of oxygen isotope ratios of coccolith calcite gathered in size-restricted microfractions to calculate SSTs (Eq. 1; see SI Materials and Methods), accounting for local seawater $\delta^{18}O$ values (6, 22) (Figs. S1 and S2) and the vital effect (19, 20) (Fig. S3). In sequences postdating the Late Miocene, large isotope vital effects have been reported in coccoliths (21). This was attributed to the consequence of relatively low pCO_2 concentrations, as DIC/CO_{2aq} limitation is thought to be the main cause of the vital effects in these biominerals (20, 21, 23–27). In contrast, studies of laboratory cultures and downcore sediments indicate that the vital effect in coccoliths (regardless of taxonomy) was limited and invariant when pCO_2 concentrations in the atmosphere were above ∼500 ppm, as was the case during the time period investigated (28, 29) (see SI Materials and Methods for further explanations on the relation between the environment and the expression of the vital effects in coccolith calcite). Beyond SST reconstruction using the oxygen isotope composition of the coccoliths, the carbon isotope offsets between coccoliths of distinct sizes, concentrated in the 5–8-μm and 3–5-μm microfractions ($\Delta\delta^{13}C_{large-small}$) can be used to derive new pCO_2 estimates that may complement existing alkenone-based data (Eq. 2; see Materials and Methods and SI Materials and Methods for details on the biogeochemical calibration for pCO_2 reconstruction).

Results

Equatorial SSTs. The new coccolith-derived SST curve at equatorial sites ODP 925 and 929 decreases across the Early to Middle Eocene transition from 38 °C to 30 °C (Fig. 1B). Middle Eocene coccoliths record temperature fluctuations of ∼4 °C from 47 Ma to 38 Ma, corroborating previous records that show an interval of climate instability (30–32) (Fig. 1B). During the Late Eocene (38 Ma to 34 Ma), the coccolith SST curve fluctuates less and exhibits a clear 6 °C warming trend. This protracted warming is distinct from the short-lived warmth at 40 Ma, commonly referred to as the Middle Eocene Climatic Optimum (MECO) (32). At the EOT, 33.7 Ma in the record, equatorial ocean temperatures were as high as they were during the late Early Eocene and subsequently underwent pronounced cooling with the development of permanent Antarctic ice sheets throughout the Early Oligocene.

From a more methodological viewpoint, we note that the use of large (5–8 μm) or small (3–5 μm) coccolith $\delta^{18}O$ values and associated treatments of the vital effects give relatively similar SST estimates (Fig. S4). Nevertheless, our SST curve is mainly based on assemblages gathered in microfractions comprised between 3 μm and 5 μm, as these fractions are purer (*Reticulofenestra*-dominated, Figs. S5–S7) and less "contaminated" by foraminiferal fragments and nannoliths such as *Discoaster* sp. that are prone to diagenesis.

The equatorial Atlantic SST estimates from the oxygen isotopes of diagenetically screened coccoliths (this study) and organic compounds (TEX$_{86}$) from the same sites exhibit similar ranges, but the trends differ (Fig. 1). Recently published SSTs derived from TEX$_{86}$ taking into account the Ring Index do not significantly vary before and across the EOT (5). The differences in SSTs in stratigraphically coeval sequences of the TDP in the Indian Ocean also remain difficult to interpret, especially as organic and inorganic-based proxy data conflict (Fig. 1A). Existing TEX$_{86}$-derived estimates for the equatorial Pacific Ocean indicate relatively colder temperatures across the EOT, but the paucity of data and the lack of record spanning the Early to Late Eocene hamper a meaningful comparison of the long- term SST trends between oceanic basins (3).

Coccolith-derived atmospheric CO$_2$ levels. The pCO$_2$ estimates obtained from coccolith inorganic δ^{13}C values of distinct sizes show a progressive and long-term decrease of about 500 ppm over the late Middle Eocene to Early Oligocene (Fig. 2). This trend corresponds to a drop of ~55 ppm of CO$_2$ per million-year period, which matches the long-term Cenozoic pCO$_2$ decline (28, 33). The atmospheric CO$_2$ concentrations presented in this study derive from concentrations of dissolved inorganic carbon (DIC) (Eq. 2; SI Materials and Methods and Figs. S8 and S9). Therefore, assumption of seawater pH (among other parameters; see SI Materials and Methods) is required to generate final atmospheric pCO$_2$ estimates and associated errors. Use of a pH value of 8.05, according to the evaluation of ref. 34 in the tropics, provides pCO$_2$ concentrations that fall within the range of previous estimates (14, 16, 28, 29, 35, 36). For reference, choosing a pH of 7.9 (37) would offset our curve by a factor of approximately +400 ppm without altering the trend (Fig. S9 C and D).

It is well established that the decrease in global temperatures that occurred during the Eocene and more broadly in the Cenozoic arose, in part, from declining pCO$_2$ concentrations (28, 38). However, in terms of rate, our Late Eocene pCO$_2$ record does not depart from this long-term overarching trend (Fig. 2). Although all previous reports agree on this decrease in pCO$_2$ during the Late Eocene, we must mention one exception to this, provided by recent work by ref. 16 showing higher Late Eocene pCO2 values than in the Middle Eocene (Fig. 2).

Discussion and implications for the long-term trigger of Antarctic glaciation

Inception of a meridional temperature gradient. The Early Eocene recorded high temperatures at both low and high latitudes (Fig. 3 A and B), providing evidence for a small meridional temperature gradient between the equator and the Southern Ocean during this interval (ΔSST < 8 °C). Such a small

temperature difference between low and high latitudes characterizes the greenhouse climate of the Early and early Middle Eocene (15, 39, 40). A low equator to subpolar temperature gradient persisted through most of the Middle Eocene, as ocean temperatures cooled at similar rates at both high and low latitudes (Fig. 3). Despite this apparently global cooling and continued decline in pCO_2, greenhouse conditions persisted during the Middle Eocene. During the late Middle Eocene and the Late Eocene, as the temperature trends diverged with low-latitude warming and accentuation of cooling in the austral subpolar regions (Fig. 3 A and B), this interval thus corresponds to the inception and progressive development of a meridional temperature gradient, at least in the Atlantic Ocean. During the latest Eocene and Early Oligocene interval, warm tropical and distinctly cooler temperatures in the sub- Antarctic regions testify to a strong latitudinal gradient (~20 °C around the EOT) akin to present-day values. Together with the development of permanent polar ice caps in Antarctica, from an oceanographic perspective, such a strong temperature gradient confirms firmly established icehouse conditions at the Eocene–Oligocene boundary.

The extent to which the Late Eocene warming was emplaced in all equatorial regions remains difficult to establish. Indeed, no reliable equatorial SSTs exist for the Pacific Ocean, and the TDP data are too patchy for the Late Eocene to exhibit a possible warming stage of the tropics of the Indian Ocean (Fig. 1A). The Oi 1 isotopic event (41), and more broadly the EOT interval, are often mentioned to pinpoint the major flip from greenhouse to icehouse conditions in the Cenozoic (12, 42). Our work, however, shows that this prominent climate transition was not an abrupt and sudden event but was emplaced progressively consecutive to a 4-My-long period of change in the latitudinal distribution of oceanic heat.

Major redistribution of oceanic heat during the Late Eocene. The causes of the Late Eocene oceanographic precursor to permanent Antarctic glaciation need to be discussed taking into account the documented environmental changes that occurred during the Middle Eocene–Early Oligocene interval. Two main climatic drivers are currently put forward to explain substantial polar cooling during this critical period of climate change: the decline in pCO_2 levels and the opening of new Southern Ocean gateways (9, 13, 14, 43). During the Late Eocene, pCO_2 concentrations continued to decline, an overarching phenomenon that may have contributed to reducing mean annual global temperatures (10). As the Late Eocene is not associated with increased atmospheric CO_2 concentrations (Fig. 2), reinvigorated greenhouse conditions and enhanced radiative forcing on temperatures cannot explain the equatorial warming. Rather, we suggest that the Late Eocene paleoceanographic and climatic changes are best explained by a major reorganization of ocean

circulation. During the Late Eocene, a reduced supply of southward flowing warm waters from the tropical Atlantic toward the austral subpolar regions can account for accentuated cooling of the South Atlantic and the Southern Ocean. From an oceanic viewpoint, this process would correspond to progressive latitudinal contraction of the subtropical gyre. Isotopic tracers provide evidence for major reorganization in the circulation of deep ocean waters in the late Middle Eocene (11, 12). Meanwhile, the Northern Atlantic Ocean did not experience cooling, as coeval warming during the Late Eocene was reported from site ODP 913 at 70°N (4) (Fig. 3A), which suggests thermal decoupling between the Southern Ocean and the Atlantic Ocean during the Late Eocene. It is likely that the thermal difference between the low- and high-latitude austral surface waters of the Atlantic Ocean fueled a meridional overturning circulation before the establishment of a true thermohaline circulation after the EOT (13).

Considering surface and deep ocean circulation upheaval together, the timing of such profound reorganization of oceanic currents, which began between 41 Ma and 38 Ma, is compatible with the opening of the Drake Passage (44–46). Neodymium isotope data further confirm the influx of SW Pacific surface waters through this newly opened seaway from 41 Ma onward (47). The emplacement of an Antarctic circumpolar current (ACC), in turn, led to the progressive thermal isolation of Southern Ocean and Antarctica, a phenomenon that continued as the gateways widened until the Late Oligocene (43, 46). The ACC is an efficient way to block warm surface waters entrained in subtropical gyres and reduce poleward heat transport. The intensity of the thermal isolation of Antarctica was subsequently reinforced at the Eocene−Oligocene boundary, when the deepening and widening of the Tasman ocean gateway led to permanent polar glaciation in Antarctica (13, 43, 48, 49).

Conclusions

By providing reliable coccolith-derived SSTs for the equatorial Atlantic, this study reveals a clear divergence in temperature trends between the Southern Ocean and the equatorial Atlantic Ocean during the Late Eocene. The emplacement and subsequent entrenchment of a strong Atlantic meridional temperature gradient characterize a climate shift from greenhouse and icehouse conditions (15). This prominent change and meridional ocean reorganization predated the Eocene−Oligocene climate transition by ~4 million years and was the likely consequence of the emplacement of an ACC. The opening of the Drake Passage led to major changes in ocean circulation, not only in the Southern Ocean, as previously established, but also with major consequences for the meridional Atlantic gyral and deep ocean currents. This precursor event heralding the EOT has to be

taken into account to constrain the feedback mechanisms ultimately responsible for the permanent glaciation of Antarctica (50). The transition from greenhouse to icehouse conditions and the emplacement of a meridional temperature gradient are broad and global phenomena that likely influenced the processes of oceanic versus atmospheric heat transport from the equator to the poles (15). The accuracy of climate models in reproducing the latent heat transport is currently limited by large uncertainties in existing temperatures (10, 51, 52). Better constraints on temperature evolution at low latitudes are crucial in this regard, as most latent heat and moisture originate from tropical regions. Therefore, the documentation of a prominent Late Eocene equatorial warming may further our understanding on how the Earth system shifted from a greenhouse to an icehouse world from a modeling perspective.

Materials and Methods

Ocean study sites. We studied sediment samples consisting of calcareous nannofossil oozes with variable amounts of clays recovered from sites ODP 925A and 929E in the western equatorial Atlantic (map in Fig. 1A, Inset). Over the entire study interval (50 Ma to 30 Ma using the age model by ref. 14), average carbonate content was 60 wt% (shipboard data), and the calcareous nannofossils assemblages are diverse and well preserved, whereas the foraminifera tests were systematically found to be recrystallized.

Coccolith separation and isotopic analyses: Diagenetic screening. We applied the protocol described in ref. 53, based on a cascade of microfiltering steps, to obtain size-restricted assemblages. The microfractions between 5 μm and 8 μm were dominated by large coccoliths mostly belonging to the *Coccolithus pelagicus* group, whereas the 3–5 μm microfractions were found to concentrate relatively smaller reticulofenestrid coccoliths (Figs. S6 and S7). After separation, granulometry, and hence quality and purity, of each fraction was controlled under cross-polarized light using a Zeiss Axioscope microscope under 1575× magnification. The state of preservation of the coccoliths (etching and overgrowth) was checked for all of the microfractions under SEM (Zeiss Supra 55VP) (Fig. S5). Noncoccolith particles, such as discoasters (star-shaped or rosette calcareous nannoliths particularly prone to diagenetic alteration) and foraminiferal fragments, were retained in the coarse fractions (8–20 μm) preceding the 5–8-μm and 3–5-μm microfraction steps. The so-called micarbs corresponding to undetermined micrometric crystals (53) were discarded in the finest (<3 μm) fraction.

Isotopic measurements. Oxygen and carbon isotope compositions were measured on 80 μg of microseparated sample residue reacted with purified phosphoric acid at 80 °C on a Kiel IV mass

spectrometer at Université Pierre et Marie Curie. Stable isotope values were calibrated relative to the Vienna Pee Dee Belemnite (‰ VPDB) via the NBS-19 international standard. The reproducibility of measurements is ±0.1‰ (1σ) for $\delta^{18}O$ and ±0.05‰ (1σ) for $\delta^{13}C$.

SST and pCO2 reconstructions. To convert the "coccolith $\delta^{18}O$ – seawater $\delta^{18}O$" offsets into temperature estimates, we used Eq. 1 derived from ref. 54.

$$\text{SST} = \frac{(1000 \times 18.03)}{(1000 \times \ln\left[(1000 + (1.03091 \times (\boldsymbol{\delta^{18}O_{cocco}} - \boldsymbol{{}^{18}O\ VE}) + 30.91)) / (1000 + \boldsymbol{\delta^{18}O_{sw}})\right] + 32.17)} - 273.15 \qquad [1]$$

Where SST is in degrees Celsius, $\delta^{18}O_{cocco}$ and oxygen isotope vital effect are in ‰ VPDB, and $\delta^{18}O_{sw}$ is in ‰ Vienna Standard Mean Ocean Water (VSMOW). The variables of the equation are in bold. Please refer to SI Materials and Methods for the treatment of the oxygen isotope vital effect (^{18}O VE) and the oxygen isotope composition of ancient seawater ($\delta^{18}O_{sw}$).

In the present study, we used a paleo-DIC equation derived from recent coccolithophore culture work with a geological perspective (19, 20). This proxy relies on the interspecies $\delta^{13}C$ compositions ($\Delta^{13}C_{large-small}$) of coccoliths of distinct sizes recently formalized in ref. 21. The range of measured $\Delta^{13}C_{large-small}$ in the Eocene–Oligocene sediment is within the range of cultured coccolith $\Delta^{13}C_{Cpel-Goc}$ values, and the sizes of the coccoliths considered here are similar in both the natural and laboratory studies (14). A notable advantage of the proxy is that it does not require knowledge of $\delta^{13}C$ of DIC (or CO_{2aq}), as is the case for alkenone paleo-CO_2 estimates. From the data of refs. 19 and 20 collectively shown in Fig. S8B, the equation tying $\Delta^{13}C_{Cpel-Goc}$ (hence $\Delta^{13}C_{large-small}$) to DIC levels is as follows:

$$\text{DIC} = 3759.1\ exp^{(\Delta 13C)} + 839.3, \qquad [2]$$

where [DIC] is in micromoles of carbon per kilogram of seawater, and $\Delta^{13}C = \delta^{13}C_{large} - \delta^{13}C_{small}$ is in ‰ VPDB (coccolith assemblages 5–8 μm and 3–5 μm, respectively). The variable of the equation is denoted in bold.

The obtained DIC estimates were subsequently transformed into pCO_2 estimates using Henry's law. Further details on these methods are provided in SI Materials and Methods.

1. Pearson PN, et al. (2001) Warm tropical sea surface temperatures in the Late Cretaceous and Eocene epochs. *Nature* 413(6855):481–487.

2. Pearson PN, et al. (2007) Stable warm tropical climate through the Eocene Epoch. *Geology* 35(3):211–214.

3. Liu Z, et al. (2009) Global cooling during the Eocene-Oligocene climate transition. *Science* 323(5918):1187–1190.

4. Inglis GN, et al. (2015) Descent toward the Icehouse: Eocene sea surface cooling inferred from GDGT distributions. *Paleoceanography* 30(7):1000–1020.

5. Zhang YG, Pagani M, Wang Z (2016) Ring Index: A new strategy to evaluate the integrity of TEX_{86} paleothermometry. *Paleoceanography* 31(2):220–232.

6. Lear CH, Elderfield H, Wilson PA (2000) Cenozoic deep-sea temperatures and global ice volumes from Mg/Ca in benthic foraminiferal calcite. *Science* 287(5451):269–272.

7. Hollis CJ, et al. (2012) Early Paleogene temperature history of the Southwest Pacific Ocean: Reconciling proxies and models. *Earth Planet Sci Lett* 349:53–66.

8. Plancq J, Mattioli E, Pittet B, Simon L, Grossi V (2014) Productivity and sea-surface temperature changes recorded during the late Eocene-early Oligocene at DSDP Site 511 (South Atlantic). *Palaeogeogr Palaeoclimatol Palaeoecol* 407:34–44.

9. DeConto RM, Pollard D (2003) Rapid Cenozoic glaciation of Antarctica induced by declining atmospheric CO_2. *Nature* 421(6920):245–249.

10. Caballero R, Huber M (2013) State-dependent climate sensitivity in past warm climates and its implications for future climate projections. *Proc Natl Acad Sci USA* 110(35):14162–14167.

11. Borrelli C, Cramer BS, Katz ME (2014) Bipolar Atlantic deepwater circulation in the middle-late Eocene: Effects of Southern Ocean gateway openings. *Paleoceanography* 29(4):308–327.

12. Cramer BS, Toggweiler JR, Wright JD, Katz ME, Miller KG (2009) Ocean overturning since the late Cretaceous: Inferences from a new benthic foraminiferal isotope compilation. *Paleoceanography* 24(4):PA4216.

13. Kennett JP (1977) Cenozoic evolution of Antarctic glaciation, the circum-Antarctic Ocean, and their impact on global paleoceanography. *J Geophys Res* 82(27):3843–3860.

14. Pagani M, et al. (2011) The role of carbon dioxide during the onset of Antarctic glaciation. *Science* 334(6060):1261–1264.

15. Pagani M, Huber M, Sageman B (2014) Greenhouse climates. *Treatise on Geochemistry*, eds Holland H, Turekian K (Elsevier, New York), 2nd Ed, pp 281–304.

16. Anagnostou E, et al. (2016) Changing atmospheric CO_2 concentration was the primary driver of early Cenozoic climate. *Nature* 533(7603):380–384.

17. Sexton PF, Wilson PA, Pearson PN (2006) Microstructural and geochemical perspectives on planktic foraminiferal preservation: "Glassy" versus "Frosty." *Geochem Geophys Geosyst* 7(12):Q12P19.

18. Prentice K, et al. (2014) Trace metal (Mg/Ca and Sr/Ca) analyses of single coccoliths by Secondary Ion Mass Spectrometry. *Geochim Cosmochim Acta* 146:90–106.

19. Rickaby REM, Henderiks J, Young JN (2010) Perturbing phytoplankton: response and isotopic fractionation with changing carbonate chemistry in two coccolithophore species. *Clim Past* 6(6):771–785.

20. Hermoso M, Chan IZX, McClelland HLO, Heureux AMC, Rickaby REM (2016) Vanishing coccolith vital effects with alleviated carbon limitation. *Biogeosciences* 13(1):301–312.

21. Bolton CT, Stoll HM (2013) Late Miocene threshold response of marine algae to carbon dioxide limitation. *Nature* 500(7464):558–562.

22. Tindall J, et al. (2010) Modelling the oxygen isotope distribution of ancient seawater using a coupled ocean-atmosphere GCM: Implications for reconstructing early Eocene climate. *Earth Planet Sci Lett* 292(3-4):265–273.

23. Hermoso M (2015) Control of ambient pH on growth and stable isotopes in phytoplanktonic calcifying algae. *Paleoceanography* 30(8):PA2844.

24. Hermoso M, Candelier Y, Browning TJ, Minoletti F (2015) Environmental control of the isotopic composition of subfossil coccolith calcite: Are laboratory culture data transferable to the natural environment? *GeoResJ* 7:35–42.

25. Hermoso M (2016) Isotopic record of Pleistocene glacial/interglacial cycles in pelagic carbonates: Revisiting historical data from the Caribbean Sea. *Quat Sci Rev* 137:69–78.

26. Rickaby REM, et al. (2016) Environmental carbonate chemistry selects for phenotype of recently isolated strains of *Emiliania huxleyi*. *Deep Res Part II* 127:28–40.

27. Hermoso M, et al. (2016) An explanation for the ^{18}O excess in Noelaerhabdaceae coccolith calcite. *Geochim Cosmochim Acta* 189:132–142.

28. Pagani M, Zachos JC, Freeman KH, Tipple B, Bohaty S (2005) Marked decline in atmospheric carbon dioxide concentrations during the Paleogene. *Science* 309(5734): 600–603.

29. Zhang YG, Pagani M, Liu Z, Bohaty SM, Deconto R (2013) A 40-million-year history of atmospheric CO_2. Philos *Trans A Math Phys Eng Sci* 371(2001):20130096.

30. Tripati A, Backman J, Elderfield H, Ferretti P (2005) Eocene bipolar glaciation associated with global carbon cycle changes. *Nature* 436(7049):341–346.

31. Bohaty SM, Zachos JC, Florindo F, Delaney ML (2009) Coupled greenhouse warming and deep-sea acidification in the middle Eocene. *Paleoceanography* 24(2):PA2207.

32. Bohaty S, Zachos J (2003) Significant Southern Ocean warming event in the late middle Eocene. *Geology* 31(11):1017–1020.

33. Hönisch B, et al. (2012) The geological record of ocean acidification. *Science* 335(6072):1058–1063.

34. Pearson PN, Palmer MR (1999) Middle Eocene seawater pH and atmospheric carbon dioxide concentrations. *Science* 284(5421):1824–1826.

35. Pearson PN, Foster GL, Wade BS (2009) Atmospheric carbon dioxide through the Eocene–Oligocene climate transition. *Nature* 461(7267):1110–1113.

36. Heureux AMC, Rickaby REM (2015) Refining our estimate of atmospheric CO_2 across the Eocene–Oligocene climatic transition. *Earth Planet Sci Lett* 409:329–338.

37. Pearson PN, Palmer MR (2000) Atmospheric carbon dioxide concentrations over the past 60 million years. *Nature* 406(6797):695–699.

38. Kent DV, Muttoni G (2008) Equatorial convergence of India and early Cenozoic climate trends. *Proc Natl Acad Sci USA* 105(42):16065–16070.

39. Huber M, Caballero R (2011) The early Eocene equable climate problem revisited. *Clim Past* 7(2):603–633.

40. Greenwood DR, Wing SL (1995) Eocene continental climates and latitudinal temperature gradients. *Geology* 23(11):1044–1048.

41. Miller KG, Wright JD, Fairbanks RG (1991) Unlocking the Ice House: Oligocene-Miocene oxygen isotopes, eustasy, and margin erosion. *J Geophys Res* 96(B4):6829–6848.

42. Zachos J, Pagani M, Sloan L, Thomas E, Billups K (2001) Trends, rhythms, and aberrations in global climate 65 Ma to present. *Science* 292(5517):686–693.

43. Kennett JP, Exon NF (2004) Paleoceanographic evolution of the Tasmanian seaway and its climatic implications. *The Cenozoic Southern Ocean: Tectonics, Sedimentation, and Climate Change Between Australia and Antarctica*, eds Exon N, Kennett JP, Malone MJ (Am Geophys Union, Washington, DC), pp 345–367.

44. Sijp WP, England MH (2004) Effect of the Drake Passage throughflow on global climate. *J Phys Oceanogr* 34(5):1254–1266.

45. Livermore R, Nankivell A, Eagles G, Morris P (2005) Paleogene opening of Drake Passage. *Earth Planet Sci Lett* 236(1-2):459–470.

46. Lagabrielle Y, Goddéris Y, Donnadieu Y, Malavieille J, Suarez M (2009) The tectonic history of Drake Passage and its possible impacts on global climate. *Earth Planet Sci Lett* 279(3-4):197–211.

47. Scher HD, Martin EE (2006) Timing and climatic consequences of the opening of Drake Passage. *Science* 312(5772):428–430.

48. Egan KE, Rickaby REM, Hendry KR, Halliday AN (2013) Opening the gateways for diatoms primes Earth for Antarctic glaciation. *Earth Planet Sci Lett* 375:34–43.

49. Bijl PK, et al.; Expedition 318 Scientists (2013) Eocene cooling linked to early flow across the Tasmanian Gateway. *Proc Natl Acad Sci USA* 110(24):9645–9650.

50. Coxall HK, Wilson PA, Pälike H, Lear CH, Backman J (2005) Rapid stepwise onset of Antarctic glaciation and deeper calcite compensation in the Pacific Ocean. *Nature* 433(7021):53–57.

51. Lunt DJ, et al. (2012) A model–data comparison for a multi-model ensemble of early Eocene atmosphere–ocean simulations: EoMIP. *Clim Past* 8(5):1717–1736.

52. Ladant J-B, Donnadieu Y, Dumas C (2014) Links between CO_2, glaciation and water flow: Reconciling the Cenozoic history of the Antarctic Circumpolar Current. *Clim Past* 10(6):1957–1966.

53. Minoletti F, Hermoso M, Gressier V (2009) Separation of sedimentary micron-sized particles for palaeoceanography and calcareous nannoplankton biogeochemistry. *Nat Protoc* 4(1):14–24.

54. Kim S-T, O'Neil JR (1997) Equilibrium and nonequilibrium oxygen isotope effects in synthetic carbonates. *Geochim Cosmochim Acta* 61(16):3461–3475.

55. Deconto RM, et al. (2008) Thresholds for Cenozoic bipolar glaciation. *Nature* 455(7213):652–656.

56. Shackleton NJ, et al. (1975) Paleotemperature history of the Cenozoic and the initiation of Antarctic glaciation: Oxygen and carbon isotope analyses in DSDP Sites 277, 279, and 281. *Initial Rep Deep Sea Drill Proj* 29:743–755.

57. Ehrmann WU, Mackensen A (1992) Sedimentological evidence for the formation of an East Antarctic ice sheet in Eocene/Oligocene time. *Palaeogeogr Palaeoclimatol Palaeoecol* 93(1-2):85–112.

58. LeGrande AN, Schmidt GA (2006) Global gridded data set of the oxygen isotopic composition in seawater. *Geophys Res Lett* 33(12):L12604.

59. Dunkley Jones T, et al. (2008) Major shifts in calcareous phytoplankton assemblages through the Eocene-Oligocene transition of Tanzania and their implications for low- latitude primary production. *Paleoceanography* 23(4):PA4204.

60. LeGrande AN, Schmidt GA (2011) Water isotopologues as a quantitative paleosalinity proxy. *Paleoceanography* 26(3):PA3225.

61. Dudley W, Blackwelder P, Brand L, Duplessy J-C (1986) Stable isotopic composition of coccoliths. *Mar Micropaleontol* 10(1-3):1–8.

62. Ziveri P, et al. (2003) Stable isotope "vital effects" in coccolith calcite. *Earth Planet Sci Lett* 210(1-2):137–149.

63. Ziveri P, Thoms S, Probert I, Geisen M, Langer G (2012) A universal carbonate ion effect on stable oxygen isotope ratios in unicellular planktonic calcifying organisms. *Biogeosciences* 9(3):1025–1032.

64. Candelier Y, Minoletti F, Probert I, Hermoso M (2013) Temperature dependence of oxygen isotope fractionation in coccolith calcite: A culture and core top calibration of the genus *Calcidiscus*. *Geochim Cosmochim Acta* 100:264–281.

65. Hermoso M, Horner TJ, Minoletti F, Rickaby REM (2014) Constraints on the vital effect in coccolithophore and dinoflagellate calcite by oxygen isotopic modification of seawater. *Geochim Cosmochim Acta* 44:612–627.

66. Stevenson EI, et al. (2014) Controls on stable strontium isotope fractionation in coccolithophores with implications for the marine Sr cycle. *Geochim Cosmochim Acta* 128:225–235.

67. Ennyu A, Arthur MA, Pagani M (2002) Fine-fraction carbonate stable isotopes as indicators of seasonal shallow mixed-layer paleohydrography. *Mar Micropaleontol* 46(3-4):317–342.

68. Hermoso M (2014) Coccolith-derived isotopic proxies in palaeoceanography: where geologists need biologists. *Cryptogam Algol* 35(4):323–351.

69. Rousselle G, Beltran C, Sicre M-A, Raffi I, De Rafélis M (2013) Changes in sea-surface conditions in the Equatorial Pacific during the middle Miocene–Pliocene as inferred from coccolith geochemistry. *Earth Planet Sci Lett* 361:412–421.

70. Henderiks J, Pagani M (2008) Coccolithophore cell size and the Paleogene decline in atmospheric CO_2. *Earth Planet Sci Lett* 269(3-4):576–584.

71. Watkins JM, Nielsen LC, Ryerson FJ, DePaolo DJ (2013) The influence of kinetics on the oxygen isotope composition of calcium carbonate. *Earth Planet Sci Lett* 375:349–360.

72. Watkins JM, Hunt JD, Ryerson FJ, DePaolo DJ (2014) The influence of temperature, pH, and growth rate on the $\delta^{18}O$ composition of inorganically precipitated calcite. *Earth Planet Sci Lett* 404:332–343.

73. Ridgwell A (2005) A Mid Mesozoic Revolution in the regulation of ocean chemistry. *Mar Geol* 217(3-4):339–357.

74. Stoll HM (2005) Limited range of interspecific vital effects in coccolith stable isotopic records during the Paleocene-Eocene thermal maximum. *Paleoceanography* 20(1): PA1007.

75. Bolton CT, Stoll HM, Mendez-Vicente A (2012) Vital effects in coccolith calcite: Cenozoic climate-pCO2 drove the diversity of carbon acquisition strategies in coccolithophores? *Paleoceanography* 27(4):PA4204.

76. Zeebe RE, Wolf-Gladrow D (2001) *CO₂ in Seawater: Equilibrium, Kinetics, Isotopes* (Elsevier, New York).

77. Robbins LL, Hansen ME, Kleypas JA, Meylan SC (2010) CO2calc—A user-friendly sea- water carbon calculator for Windows, Max OS X, and iOS (iPhone). *US Geol Surv Open File Rep* 2010-1280:1–18.

78. Holtz L-M, Wolf-Gladrow D, Thoms S (2015) Numerical cell model investigating cellular carbon fluxes in *Emiliania huxleyi*. *J Theor Biol* 364:305–315.
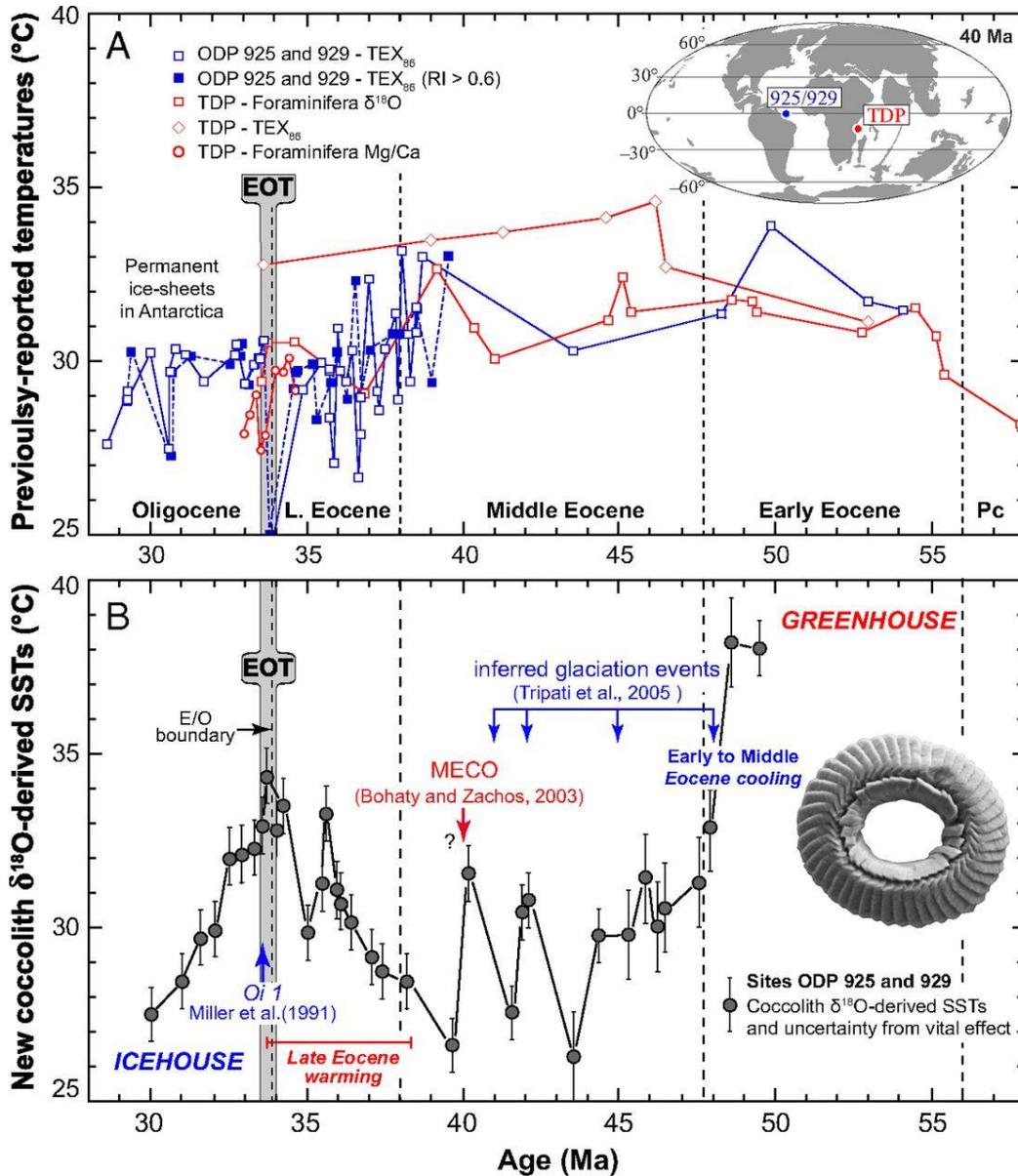
Fig. 1. Reconstructed equatorial SSTs during the Early Eocene to the Early Oligocene. (A) Multiproxy temperature estimates from the TDP (in red) indicate a warm and relatively stable Eocene climate (2). The blue curve denotes published TEX$_{86}$-derived SSTs (3, 4) in the equatorial Atlantic showing relatively similar temperatures in the Eocene and the Early Oligocene. Note that alkenone temperatures (U$^{K'}_{37}$) from ref. 3 are not presented, as they exceeded the upper limit of the proxy (i.e., >29 °C). For data source ODP 925 and 929, open symbols denote refs. 3 and 4, and filled symbols denote samples with a Ring Index > 0.6 from ref. 5; TDP data are from refs. 2 and 35. (Inset)

The location map is modified from ref. 29. (B) Coccolith $\delta^{18}O$-derived temperatures from sites ODP 925 and 929 applying Eq. 1. The raw isotope data are shown in Fig. S4A. A correction of the vital effect of 0.69‰ (SD = 0.11‰) was applied to coccoliths gathered into 3–5 µm fractions (see corresponding biogeochemical discussion in SI Materials and Methods). Disregarding the problem of the vital effect would translate the temperature curve by a constant −3.7 °C offset (see Fig. S4D for SSTs derived from the 5–8 µm fractions). Early to Middle Eocene cooling highlights the termination of the greenhouse period. After climate ups and downs in the Middle Eocene (30–32), including the Middle Eocene Climatic Optimum (MECO), a Late Eocene 6 °C warming predates the pronounced cooling seen coeval with the onset of glaciation during the Early Oligocene. (Inset) The SEM image shows a reticulofenestrid specimen from a sample at 42.1 Ma (see Fig. S5A for an edited version and the scale bar).
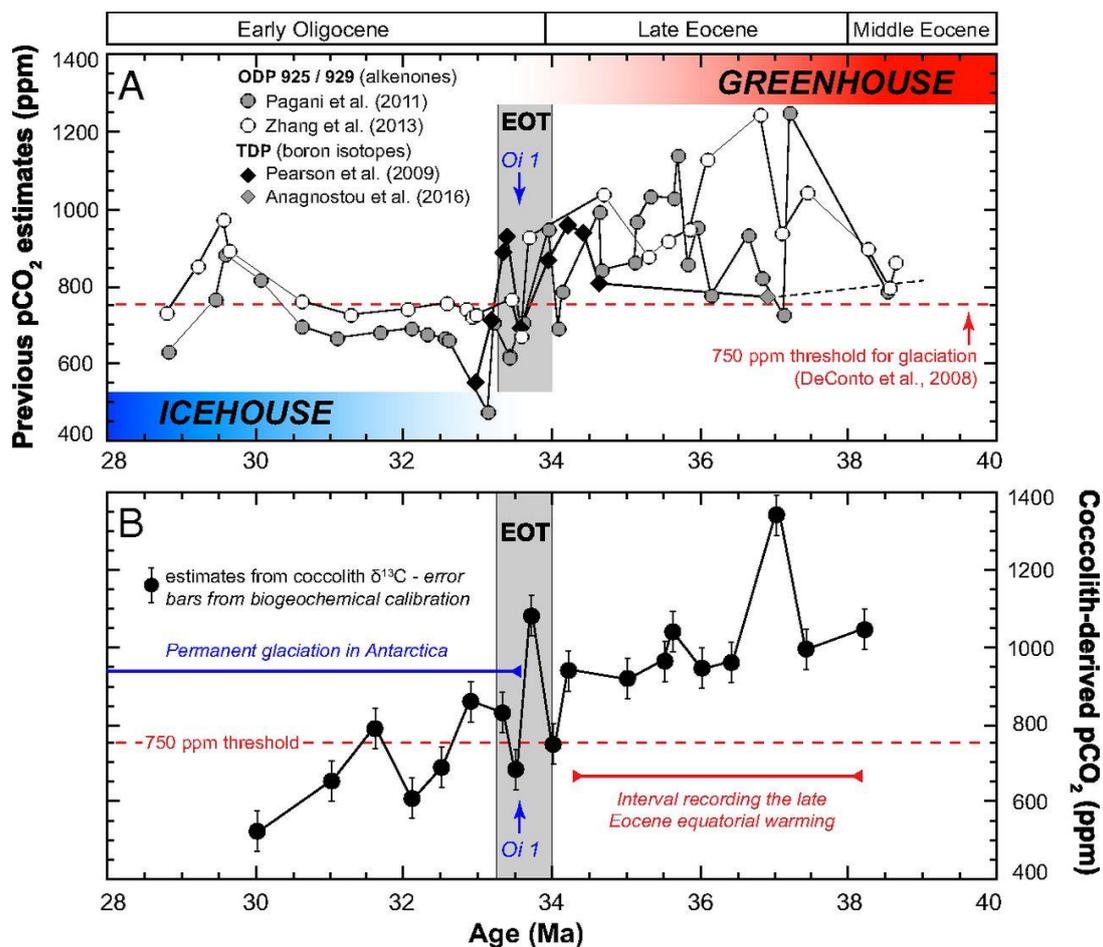

Fig. 2. Evolution of atmospheric carbon dioxide concentrations during the Middle Eocene to Early Oligocene. (A) Previously reported data indicating a decline in pCO_2 throughout the study interval (14, 16, 29, 35). Note that the data from ref. 35 established from boron isotope composition of foraminifera from the TDP (solid diamonds) are those recently reevaluated by ref. 16. (B) Our pCO_2

coccolith-derived estimates with the pH assumed to be 8.05 (according to ref. 34) are compatible with previous reports, but they reveal a clear and a more progressive negative trend. The Late Eocene warming (Fig. 1B) does not coincide with pCO_2 upheaval compared with a long-term record that would indicate fleeting reestablishment of the greenhouse period. Across the EOT (gray shaded area), these estimates are compatible with the modeled pCO_2 threshold at 750 ppm, compatible with glaciation in Antarctica (55).
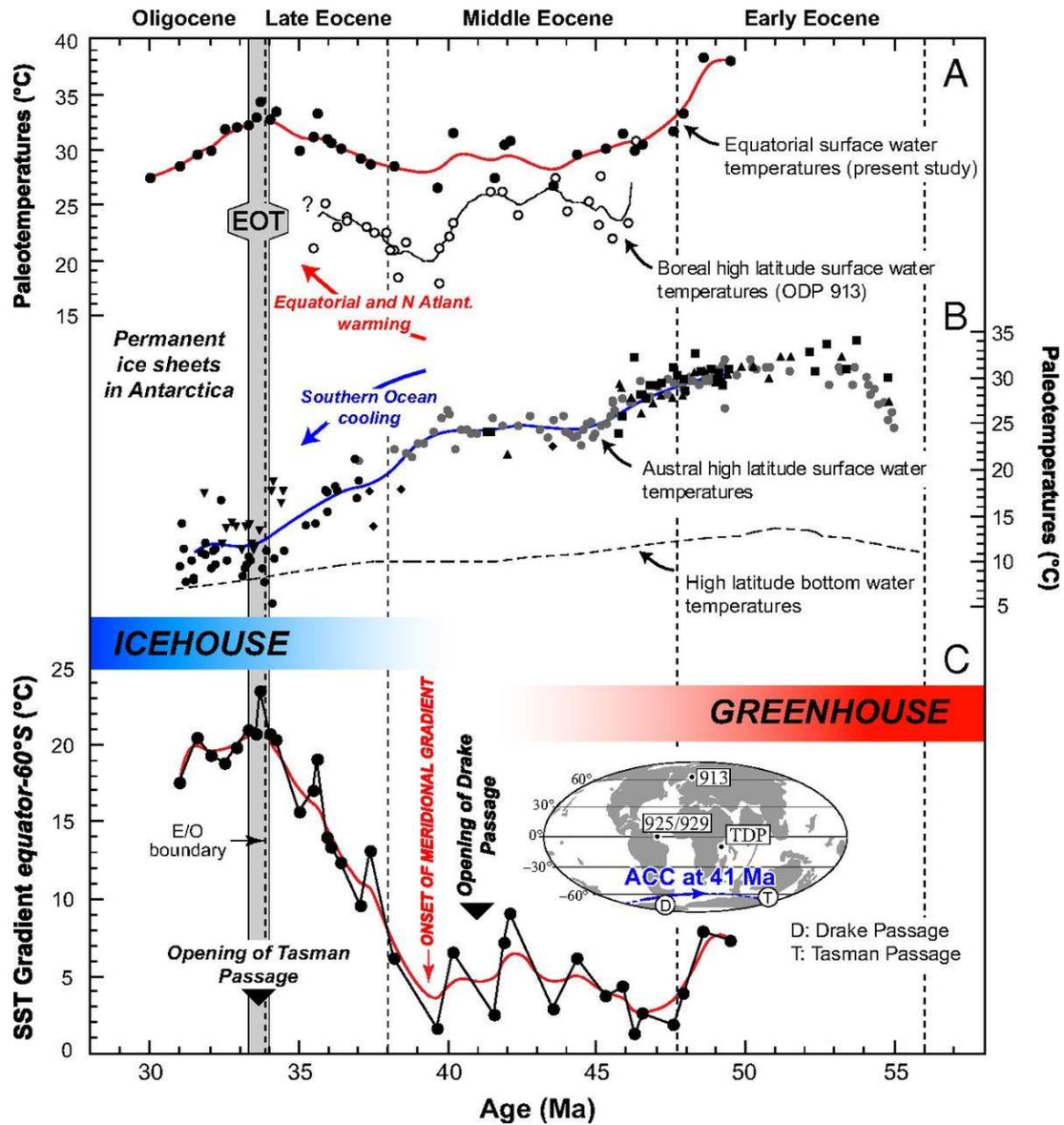
Fig. 3. Meridional temperature gradient revealing the shift from greenhouse to icehouse conditions leading to the EOT. (A) Equatorial [ODP 925 and 929 (present study)] and sub-Arctic [ODP 913 (4)] SSTs show similar warming from 38 Ma to 40 Ma. (B) SST estimates from southern high-latitude sites exhibited more pronounced austral subpolar cooling from 40 Ma (data from refs. 4 and 8). High-

latitude bottom water temperatures are from ref. 6. (C) Evolution of the meridional (surface) temperature gradient calculated as the SST difference between the equatorial Atlantic and Southern Oceans. The onset of this gradient, linked to the initiation of ACC, highlights the transition from greenhouse to icehouse, leading to permanent ice sheets on Antarctica after the OI 1 event (41).

Supporting Information

SI Materials and Methods

Constraints on local seawater oxygen isotope ratios over the studied interval. Generating SST estimates from the oxygen isotope composition of coccolith calcite requires knowledge of the oxygen isotope ratio of seawater ($\delta^{18}O_{sw}$). The reconstruction of $\delta^{18}O_{sw}$ values in deep time is not straightforward and relies on a number of assumptions about the oxygen isotope budget of the global ocean (primarily linked to ice volume) and the effect of the hydrographic regime of the considered area, here the western equatorial Atlantic Ocean. In this study, we use published data (6, 22, 56) to determine, independently of any interpretation relying on our final SST estimates, the absolute values of $\delta^{18}O_{sw}$ in the equatorial Atlantic surface waters where the coccoliths have calcified. As it is essential to ensure our reconstructed SST do not reflect the imposed variations in $\delta^{18}O_{sw}$, we will assess the effect of this parameter in the paleotemperature curve over the Early Eocene to Early Oligocene interval.

Over the Meso-Cenozoic, the isotopic ratio of the world ocean ($\delta^{18}O_{sw}$ "global") has primarily evolved as a function of ice volume, and thus has fluctuated between ice-free values of −1.0‰ VSMOW (56) and values closer to zero during periods with more or less developed continental ice sheets, leaving relatively ^{16}O-depleted oceanic waters [0‰ VSMOW in present days (56)]. During the Paleogene, $\delta^{18}O_{sw}$ values fluctuated between −1‰ and −0.3‰ (6). Our study interval comprises periods characterized by ice-free oceans in the Early Eocene, by small and/or transient ice caps in the Middle and Late Eocene, and by permanent glaciation during and after the EOT (6, 12, 30) (Fig. S1). Proxies for assessing global ocean $\delta^{18}O_{sw}$ include paired Mg/Ca and $\delta^{18}O$ measurements from benthic foraminifera from high southern latitude sites (6), which are driven by deep waters formed from the downwelling of southern ocean surface waters (11). Mg/Ca ratios are used to independently assess temperature of calcification of foraminiferal tests and isolate the respective effect of temperature and $\delta^{18}O_{sw}$ variations from foraminiferal $\delta^{18}O$ composition. Global ocean $\delta^{18}O_{sw}$ evolved from ice-free values (−1.0‰ VSMOW) before the Middle Eocene toward near-zero isotope ratios, thus describing

an overarching positive trend during the study interval (Fig. S1). In the Middle and Late Eocene, minor and only fleeting excursions of about +0.3‰ to +0.4‰ are recorded, corresponding to ephemeral ice sheets, which are also inferred from sedimentological evidence (refs. 30 and 57 and references therein). The EOT is marked by a sharp ~1‰ increase ("Oi 1," ref. 41), followed by a decrease of 0.4‰ during the earliest Oligocene (from 32.9 Ma to 31 Ma), an evolution that matches the established onset of permanent ice cap on Antarctica and its subsequent partial melting in the earliest Oligocene, respectively (12).

In the present study, SSTs are calculated by using local surface water $\delta^{18}O_{sw}$ in the equatorial Atlantic. Therefore, the global ocean value of ref. 6 needs to be corrected by the offset of equatorial Atlantic values from global ocean values. This offset, primarily controlled by the regional evaporation to precipitation ratio, has been quantified for the Early Eocene (22). According to this modeling experiment, surface waters at the equatorial Atlantic are enriched in heavy oxygen isotopes (+1‰ ± 0.2‰) due to more evaporated waters compared with the global ocean, as is still the case in present-day settings (58). Therefore, an equatorial Atlantic $\delta^{18}O_{sw}$ value of 0‰ (±0.2‰) is suitable for the Early Eocene. For youngest intervals in our sites, we derived local $\delta^{18}Os_w$ estimates by taking the global ocean $\delta^{18}O_{sw}$ curve of ref. 6 offset by the afore-mentioned coefficient (22) (Fig. S1).

To date, the only studies that have used tropical $\delta^{18}O$ values to derive Paleogene SSTs are from the Tanzanian sites (TDP) (1, 2, 59), but they predate the insightful modeling work by ref. 22 that allowed refinement in $\delta^{18}O_{sw}$ estimates. The Early Eocene local value of −0.75‰ used by ref. 2 for the TDP corresponds to an ice-free ocean (−1‰, according to ref. 6) and an offset from global ocean of +0.25‰, which agrees with ref. 22. For the Middle and Late Eocene, global ocean $\delta^{18}O_{sw}$ values fluctuated between −1‰ and −0.6‰. By applying the same offset for our studied location, local values are thus comprised between −0.75‰ and −0.35‰. It is worth noting that the figure of −0.5‰ used by ref. 2 for the Middle and Late Eocene is consistent with the mean value for this interval. Consequently, the values used in the present study and in ref. 2 are in line with recent evaluations of refs. 6 and 22. The differences between previously reported SSTs inferred from TDP foraminiferal $\delta^{18}O$ and the new estimates from coccolith $\delta^{18}O$ at sites ODP 925 and 929 cannot therefore arise from distinct treatment or uncertainties in the $\delta^{18}O_{sw}$ used to calculate temperature estimates.

Coccolith $\delta^{18}O$ compositions used to calculate SSTs are concurrently dictated by the temperature of calcification, the signal sought in our approach, and $\delta^{18}O_{sw}$ values of the mineralizing fluid (see Coccolith Oxygen Isotopes and SST Reconstructions for the vital effect problem). To verify that the weight of $\delta^{18}O_{sw}$ fluctuations in our temperature curve is only minor, we deconvolved the

relative effect of temperature and $\delta^{18}O_{sw}$ by using an incremental approach between consecutive samples. Overall, there is no correlation between ΔSST and $\Delta\delta^{18}O_{sw}$ increments (r^2 = 0.018 and P value = 0.48). The effect of $\delta^{18}O_{sw}$ change on temperature increments can be obtained via the slope of equation tying temperature and oxygen isotope ratios (−0.2‰/°C after ref. 60) and enables us to express $\delta^{18}O_{sw}$ variations in a temperature framework (which indicate a conservative temperature effect of 1.4 °C). Therefore, we can confidently assess that there is no influence of the $\delta^{18}O_{sw}$ values on our final SST estimates (Fig. S2). More specifically, the magnitude of temperature changes across the Early to Middle Eocene (cooling) and late Middle Eocene to the EOT (warming) cannot be the result of the imposed $\delta^{18}O_{sw}$. For the latter event, which is the key finding of the present study, it further appears that the applied $\delta^{18}O_{sw}$ change would, in fact, underevaluate the +6 °C warming.

Background information on coccolith biogeochemistry and the vital effects. Following on from the pioneering work by Dudley et al. (61), 30 years of research on the biogeochemistry of the coccolithophores have led to a better understanding of the mechanisms responsible for the isotopic departure of coccoliths from inorganically precipitated calcite, the so-called "vital effect." A series of cultures of these phytoplanktonic calcifiers in the laboratory have provided empirical calibrations and a mechanistic understanding of the vital effect that allow circumventing this classical problem in paleoceanography. Furthermore, these studies have progressively highlighted the potential of these biominerals to decipher paleoenvironments in complement to the foraminiferal archive (19–21, 23, 27, 62–66). Examining geologically relevant coccolithophore species exposed to a wide range of ambient DIC concentrations/pCO$_2$, a relaxation of the expression of the vital effects, imprinting both carbon and oxygen isotope systems, has become apparent (19, 20, 23). Diminished vital effects are thought to be the result of alleviated carbon limitation that arguably exists in the aforementioned cultures implemented at present-day and under post-Miocene pCO$_2$ values (20, 21, 23, 25, 27, 65, 67–69). The concept of environmentally driven vital effects (68) is able to reconcile culture and natural environment data and, as such, provides valuable insights in paleoceanography.

Using culture data on extant species, we formalize here a calibration between coccolith calcite $\delta^{18}O$ values and temperature, on one hand, and $\delta^{13}C$ and DIC/pCO$_2$ levels, on the other hand. Overall, it appears that the coccolith proxies rely on the distinct size of coccolith, and therefore that of the cell, rather than on true interspecies differences. Based on these morphological (size) grounds, the species that serve as analogs of ancient coccoliths encountered in sites ODP 925 and 929 sediments are *Gephyrocapsa oceanica*, representing the descendant of *Reticulofenestra* coccoliths within the Noelaerhabdaceae lineage, and *C. pelagicus*, representing the *Coccolithus* group. The sizes

of these modern forms of coccoliths indeed fall within a 3–5-μm and 5–8-μm range, respectively (14, 70). We must note that *G. oceanica* has usually slightly smaller cell than *Reticulofenestra* and, as such, may have a lower carbon demand than its ancestors. This difference in cell volume to surface-area ratio would require size normalization of the vital effect. However, it appears that reticulofenestrid coccoliths retrieved from equatorial sites exhibit very similar sizes to cultured *G. oceanica*, with only small variations (14); therefore, such a correction was not applied in the present study.

Coccolith oxygen isotopes and SST reconstructions.

Biogeochemical calibration. Most modern coccolith species precipitate calcite away from equilibrium conditions in the oxygen isotope system, as a result of carbon limitation (54, 71, 72). The range of interspecific coccolith $\delta^{18}O$ has been found to be considerable in culture (on the order of 4‰). The Paleogene, however, temporally predates the "Late Miocene threshold" (21) and elevated pCO_2 levels induced much more limited oxygen vital effects (Fig. S3). Overall, the culture datasets (19, 20) indicate that a coccolith-integrated coefficient of the vital effect between 0.4‰ and 0.9‰ would need to be applied in Eq. 1 (see Materials and Methods) to transform coccolith $\delta^{18}O$ values into SST estimates under a high pCO_2 regime. We can calculate a residual oxygen isotope vital effect at pCO_2 higher than 500 ppm for each species. For *Coccolithus* coccoliths, it is 0.51‰ ± 0.15‰, and, for *Reticulofenestra* coccoliths, it is 0.69‰ ± 0.11‰. These SDs would indicate an uncertainty in coccolith $\delta^{18}O$-derived SST estimates less than 0.8 °C for both species (see below).

Another possible uncertainty in our paleo-vital effect calibration pertains to seawater pH. Indeed, the proposed pH values for the Paleogene ocean are lower than today's values, as a consequence of higher pCO_2 levels (34, 73). The two coccolithophore species serving here as reference have been grown over a wide range of medium pH, and their $\delta^{18}O$ analyzed (23). There was no apparent effect on *C. pelagicus*, which consistently exhibits $\delta^{18}O$ values close to inorganic calcite reference, but, for *G. oceanica*, in contrast, $\delta^{18}O$ values decreased by a factor of ~0.5‰ from pH 8.2 to 7.4. Bearing in mind that these culture data were obtained at the present-day pCO_2 level, it can arguably be conceived that decreased oxygen isotope vital effect in the laboratory is the consequence of elevated CO_{2aq} at low pH (23). Therefore, we did not apply any pH correction on the stable isotope compositions of Paleogene *Coccolithus* and *Reticulofenestra* coccoliths.

Sedimentary data also confirm diminished expression of the oxygen isotope vital effect in coccolith calcite compared with present-day (relatively low pCO_2) settings, as the range of $\Delta^{18}O_{foraminifera-coccolith}$ offset was only minor during the Paleogene (53, 74, 75). A downcore Pleistocene record (therefore postdating the Late Miocene) provides a paleo-vital effect framework for gephyrocapsid coccoliths and confirms the pCO_2 dependence of the oxygen isotope vital effect (25). By extrapolating the oxygen isotope vital effect above a pCO_2 value of 500 ppm, it would appear that this isotopic phenomenon is indeed vanished. This field validation of laboratory findings is an important aspect lending support to the robustness of the oxygen isotope paleo-vital effects applied in the present study (19, 20) and, overall, validates the fact that disregarding the vital effect in the numerous attempts to reconstruct SST from bulk or sediment fine fraction $\delta^{18}O$ in the Jurassic, Cretaceous, and Paleogene worlds seems to be justified.

Error on SST figures. Each variable parameter used in Eq. 1 needs to be associated with a specific error, and a cumulative and propagated uncertainty in our SST estimates ought to be calculated (Fig. S4). For coccolith calcite $\delta^{18}O$ measurement, the analytical error is 0.1‰ VPDB. For seawater $\delta^{18}O$, it is 0.2‰ VSMOW (see Constraints on Local Seawater Oxygen Isotope Ratios over the Studied Interval). The SD of the oxygen isotope vital effect (^{18}O VE) is 0.11‰ for Reticulofenestra. The error associated with the vital effect free $\delta^{18}O$ (i.e., the "$\delta^{18}O_{coccolith} - {}^{18}O$ VE" term in Eq. 1) is $\sqrt{(0.1^2 + 0.11^2)}$, hence 0.15. When the extremes of each individual variable are propagated through Eq. 1, it then appears that the conservative uncertainty in SST reconstruction is on the order of 1.6 °C (the error bars reported in Fig. 1B).

The SST estimates presented in this study derive from well-preserved (reticulofenestrid) coccoliths (Figs. S5–S7), and, especially, they are barren of calcite overgrowth, implying that they convey a pristine $\delta^{18}O$ record. Some coarser particles, however, may pervade into the 3–5-µm assemblages due to imperfections in the screen membranes used (see details in ref. 53). In all of the 3–5 µm fractions presented in the present study, the calcite mass of the fraction is composed by, at least, 90 wt% of coccolith calcite (Figs. S6 and S7). Assuming a conservative "contamination" of the 5–8 µm fractions, the $\delta^{18}O$ of which is known, we can, by a simple mass balance equation, assess the effect of this purity on our final SSTs. Overall, this effect is only minor, as one may expect on the basis of similar $\delta^{18}O$ values observed between the 3–5 µm and 5–8 µm fractions and relative similar vital effects applied to *Gephyrocapsa* and *Coccolithus* coccoliths (Fig. S4E).

Formalizing a CO_2 proxy based on coccolith carbon isotopes.

Interspecies Δ^{13}C offset and ambient CO_2 (DIC) levels. The pCO_2 proxy presented here (Eq. 2) is based on a compilation of data from two distinct laboratory culture studies performed on different strains of *G. oceanica* and *C. pelagicus* (19, 20) (Fig. S8A). These studies have examined the evolution of coccolith δ^{13}C under a wide range of pCO_2/DIC levels compatible with Paleogene and Neogene values. Interspecific δ^{13}C composition of coccoliths is primarily the result of differences in the volume to surface-area ratios (themselves scaling cell size) in coccolithophores. These parameters (among others) control carbon limitation and ultimately dictate the magnitude of the vital effect (20, 21). We note that the size of the cultured *G. oceanica* coccoliths and that of sedimentary specimens gathered into size fractions at site ODP 925 are similar (14); the same observation applies for *Coccolithus*, thus providing a suitable culture-based calibration for our study case.

From seawater DIC estimates to atmospheric CO_2 concentrations. In seawater, the concentration of DIC is conservative, meaning that the total amount of inorganic carbon species is not temperature-or pH-dependent, in contrast to aqueous CO_2 concentrations (CO_{2aq}). We then need to account for the following parameters (76) to generate atmospheric pCO_2 estimates, noting that points *i* and *iii* are common with the alkenone-based proxy: (*i*) temperature and salinity, as they set the exchange between CO_{2g} and CO_{2aq} and between dissolved DIC species; (*ii*) seawater pH values, as they set the relative proportion of CO_{2aq} with respect to DIC; and (*iii*) the air–surface ocean disequilibrium at the considered paleolocation.

Using the CO_2CALC software (77), we converted our DIC estimates into atmospheric CO_2 concentrations assuming a range of pH between 7.9 and 8.05, as per refs. 34 and 73, using the temperatures from our SSTs derived from coccolith δ^{18}O values (Fig. 1B), and assuming a constant salinity of 35 (Fig. S9 C and D). Last, according to ref. 29, the surface ocean water mass was at near-equilibrium with the atmosphere at sites ODP 925 and 929, so we did not apply any final correction. Compared with the alkenone-based CO_2 barometry, we do not make an assumption about the relative contribution of CO_2 and HCO_3^- to photosynthetic carbon fixation; as for calcification, HCO_3^- (hence DIC) is the ultimate carbon substrate used by the coccolithophores to calcify (78).

Cumulative errors on pCO_2 estimates. The error bars reported on the pCO_2 estimates (Fig. 2B) denote the cumulative error associated with the biogeochemical calibration (taking the confidence limits of the exponential function), uncertainty in SST estimates (seawater δ^{18}O values are given ±0.2‰ VSMOW after ref. 22), and the analytical error in the δ^{13}C measurement [$\sqrt{(0.05^2 + 0.05^2)}$ = 0.07‰ VPDB]. The uncertainty in our DIC evaluation is thus rather small (<75 ppm) and has little effect on our pCO_2 reconstruction. It corresponds, on average, to less than 9% of the reconstructed values. The effect of uncertainty in temperature (±0.8 °C) is negligible (<10 ppm). Consequently, the

curves describing paleo-CO_2 and paleo-DIC estimates are broadly parallel (Fig. S9 C and D), the latter being uninfluenced by external parameters (SST) of the calibration. This point is of particular importance in our study, considering that we compare our new pCO_2 and SSTs, and thus avoid circularity. The temperature effect in our pCO_2 estimates is not significant (± 30 ppm over the entire studied interval), confirming that both parameters are decoupled. The effect of salinity, for reference, is small. Taking a salinity value of 33 would only affect the CO_2 values by a negligible CO_2 amount, on the order of 10 ppm, compared with the salinity of 35 taken in our derivations. In contrast, the pH effect is a much greater source of uncertainty in the final pCO_2 estimates. Rather than propagating errors bars on a favored pH assumption, we have chosen to show distinct curves in Fig. S9 C and D, either using pH 8.05 or 7.9 (34, 73).
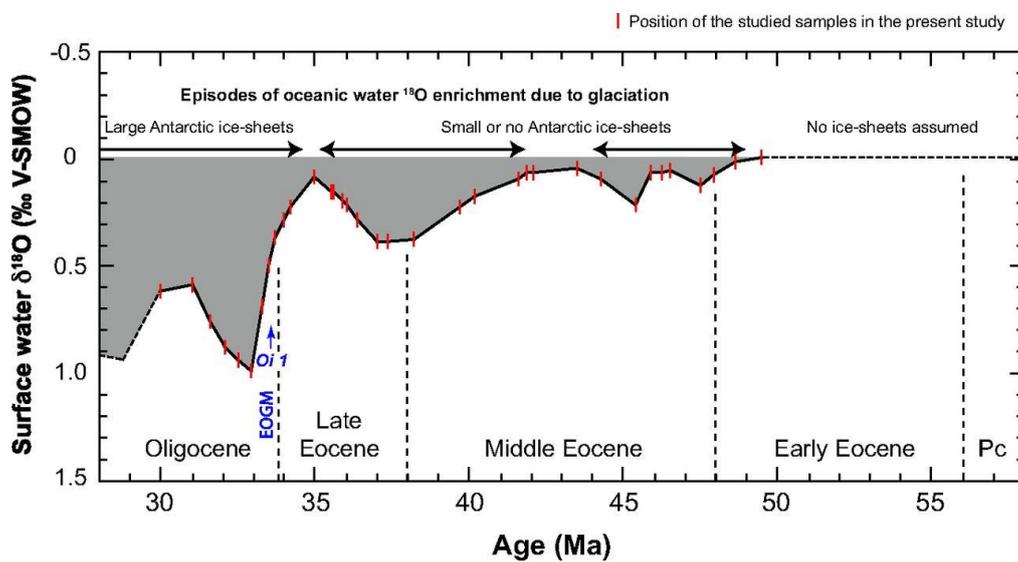
Fig. S1. Seawater oxygen isotope composition used to calculate temperature estimates in the present study. Reconstructed $\delta^{18}O_{sw}$ values are from refs. 2 and 6. EOGM, Eocene–Oligocene Glacial Maximum
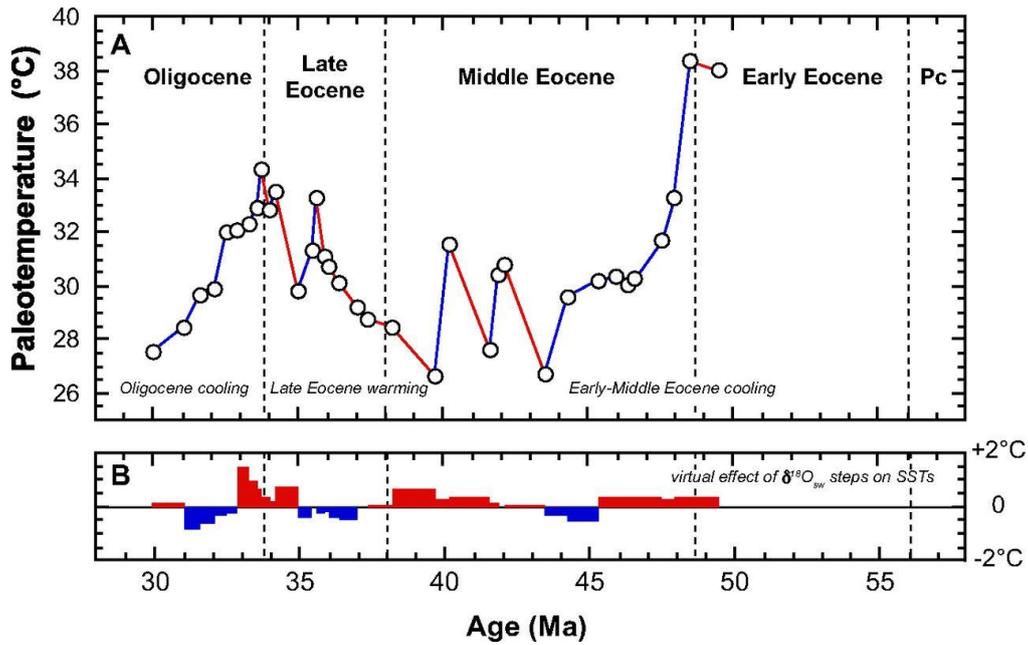
Fig. S2. A posteriori comparison between the paleotemperature estimates obtained in the present study and $\delta^{18}O_{sw}$ values used. (A) SST evolution from reticulofenestrid $\delta^{18}O$, as shown in Fig. 1B. (B) Increments in $\delta^{18}O_{sw}$ steps between two consecutive samples converted into temperature equivalents.
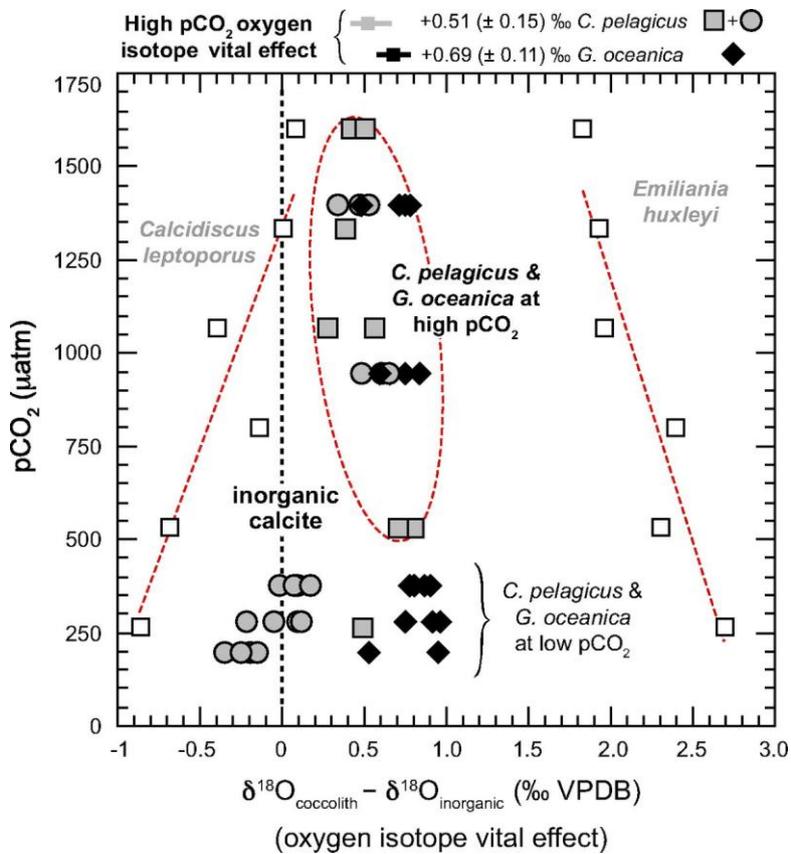
Fig. S3. Evolution of oxygen isotope vital effect (coccolith $\delta^{18}O$ offset from inorganic values) with increasing pCO_2 for *C. pelagicus* (gray symbols) and *G. oceanica* (black diamonds) in culture. Data source is ref. 19 (black diamonds and gray circles) and ref. 20 (all other datapoints). When grown at high pCO_2, the two species of interest precipitate calcite isotopically heavier than the inorganic reference (54) (vertical dashed line). *Calcidiscus leptoporus* and *Emiliania huxleyi* isotopic behaviors are indicated, for reference only, with open squares. The datapoints for *G. oceanica* and *C. pelagicus* used to calculate the magnitude of the vital effect above a 500-ppm pCO_2 threshold are circled in red.
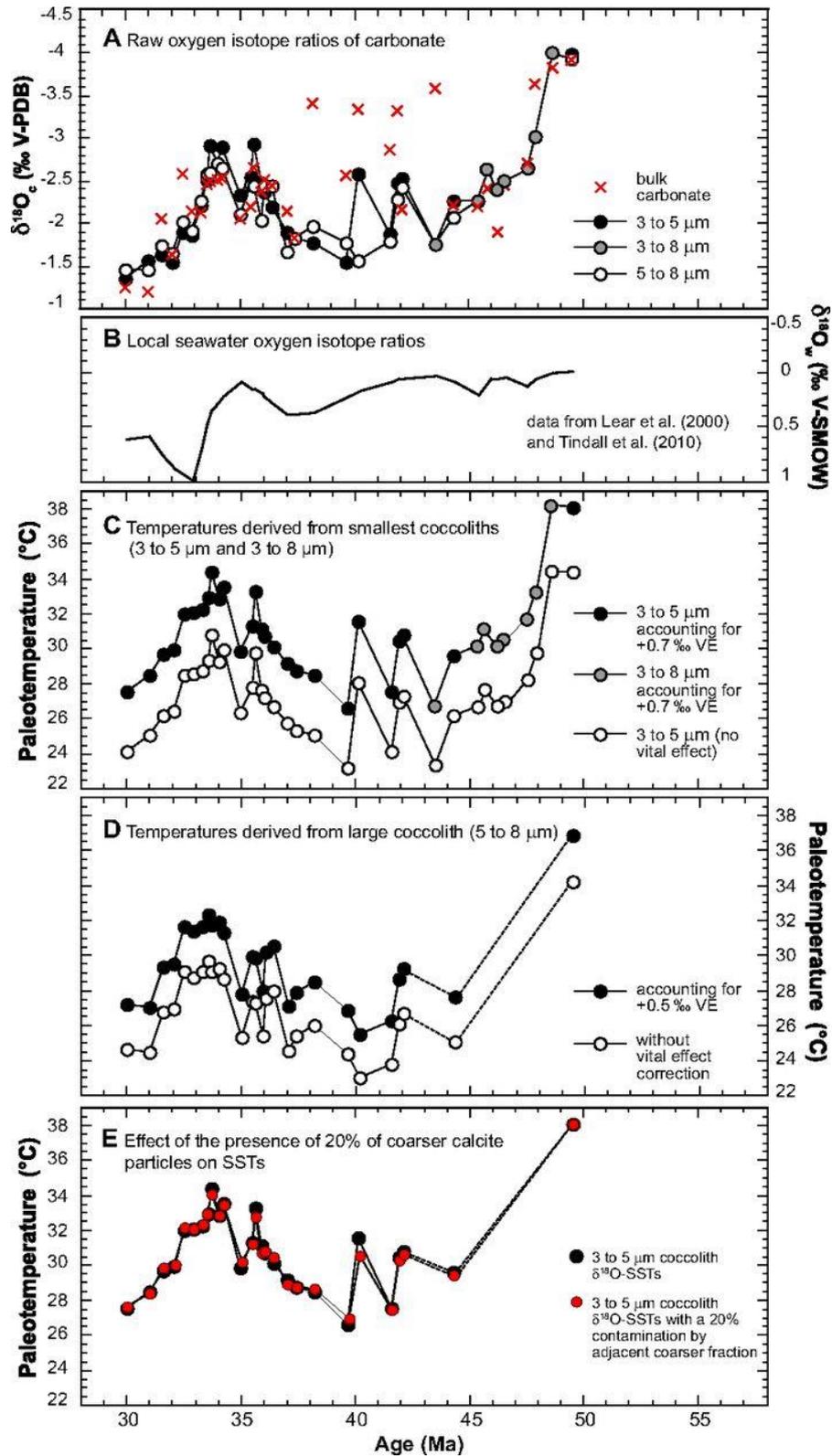
Fig. S4. (A) Raw bulk and coccolith fraction $\delta^{18}O$ values, (B) applied $\delta^{18}O_{sw}$ values (6, 22), and (C and D) comparison in the reconstructed SST estimates with correction of the vital effect for (C) small and (D) large coccoliths. (E) The negligible effect of the presence of 20% of coarser calcite particles (from

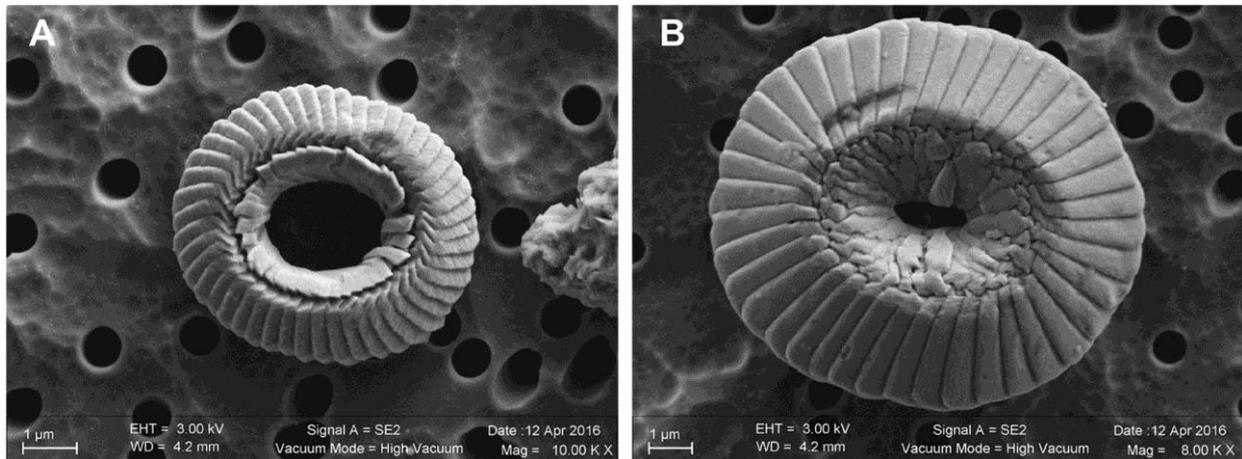the adjacent 5–8 µm fraction) on our SST reconstruction mainly based on 3–5 µm microfractions (Fig. 1B).

Fig. S5. Close-up of coccolith specimens showing the excellent preservation state of the coccoliths: (A) *Reticulofenestra* sp.sample at 42.1Ma and (B) *C. pelagicus* sample at 30.0 Ma. Slight etching of the coccoliths may be the result of the microseparation technique, but the absence of notable calcite overgrowth on the coccoliths is evident. Scale bars are inset.
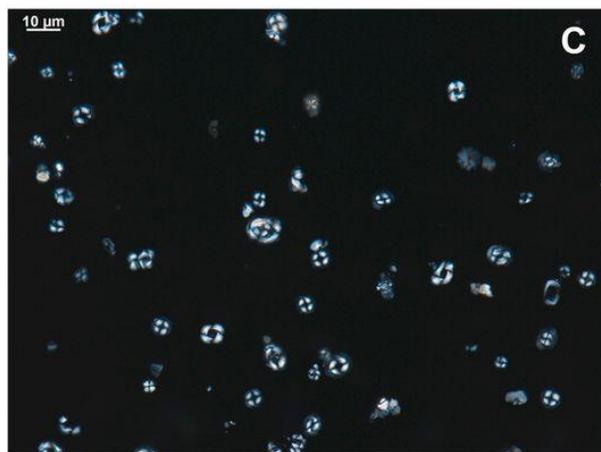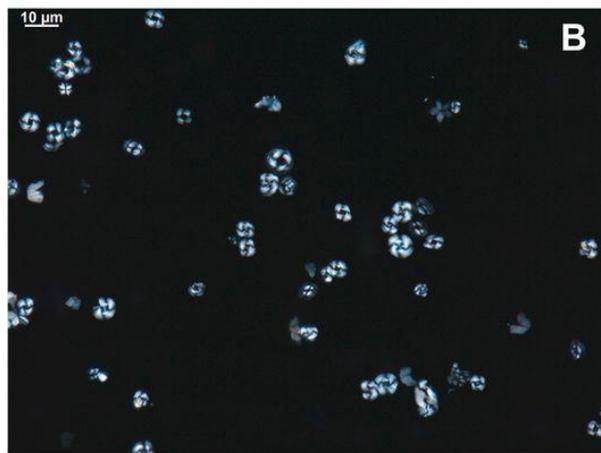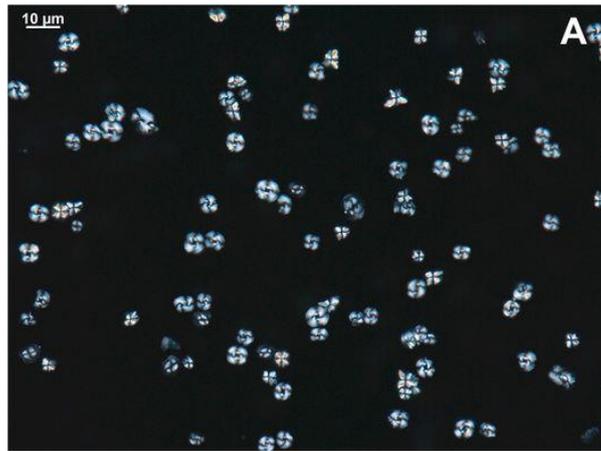
Fig. S6. Cross-polarized micrographs of 3–5 µm microseparated fractions distributed throughout the studied interval and showing a high relative abundance (>80%) of small coccoliths. (A) Oligocene sample (31 Ma). (B) Late Eocene sample (34.2 Ma). (C) Middle Eocene sample (41.9 Ma). Scale bars are inset.

Fig. S7. SEM micrograph showing the high abundance of relatively small coccoliths in the 3–5 μm microfractions (example from the Oligocene sample at 30.0 Ma). Scale bar is inset.
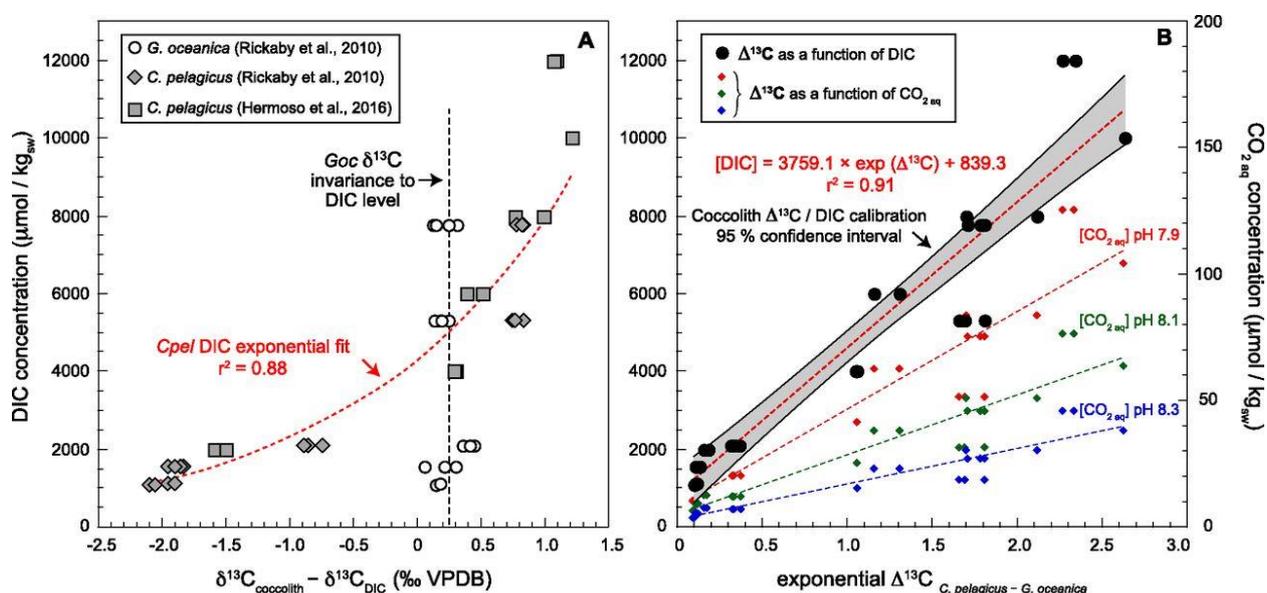

Fig. S8. Culture-derived relationship between coccolith carbon isotopes and ambient DIC levels. (A) Offset between the coccolith carbon isotope composition and that of DIC in the culture medium. (Inset) Data are from refs. 19 and 20. (B) Expression of the interspecies (intersize) correlation using an exponential fit between $\Delta^{13}C$ ($\delta^{13}C_{Cpel} - \delta^{13}C_{Goc}$) and DIC concentrations in culture medium (left vertical axis) and, for reference, ambient aqueous CO_2 (right vertical axis).

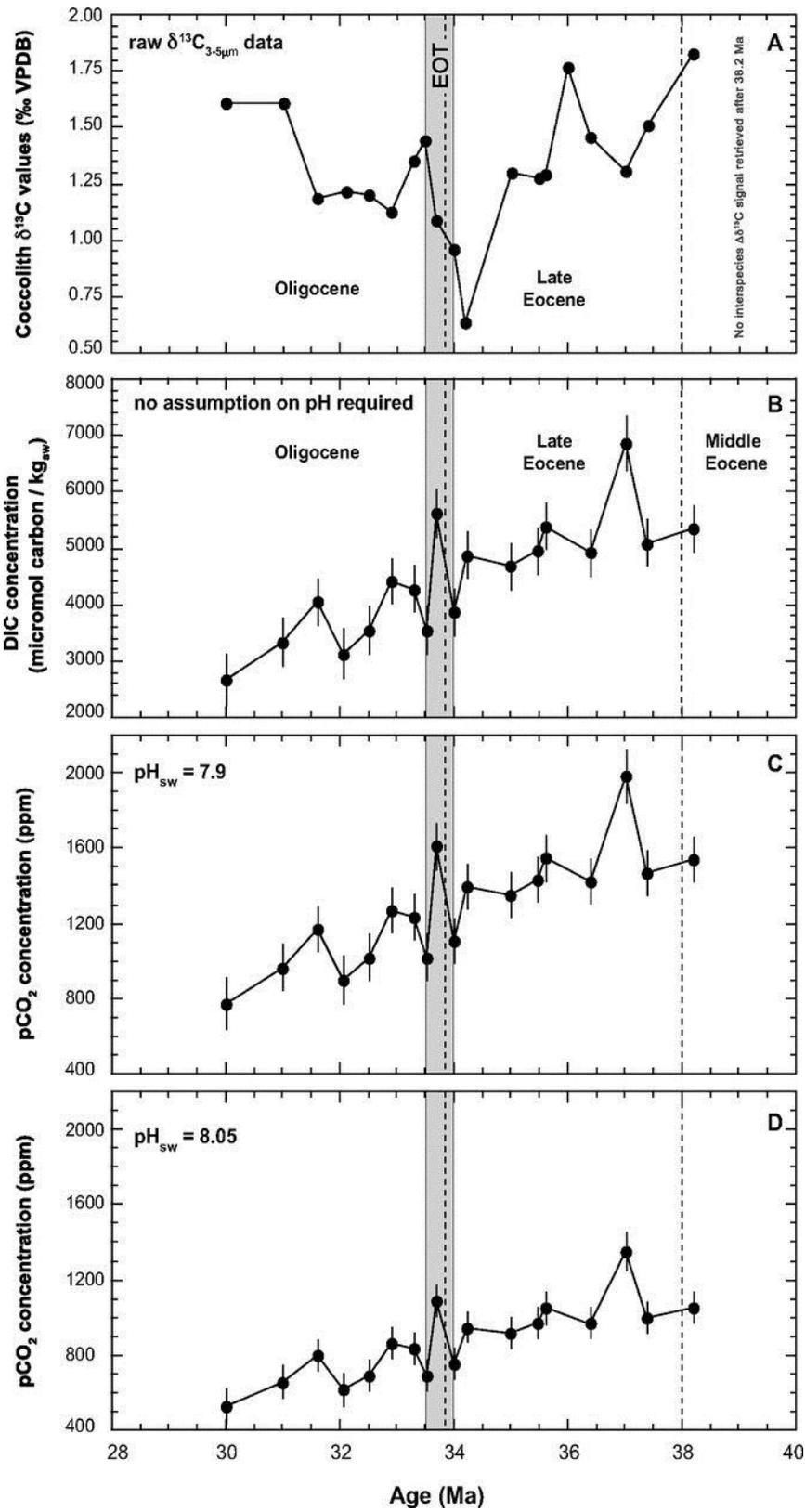**Fig. S9.** (A) Raw $\delta^{13}C$ values of the 3–5 μm coccolith microfractions, (B) comparison between the estimates of paleo-DIC concentrations from the bio-geochemical calibration, and (C and D) pCO$_2$ estimates applying two distinct seawater pH values: (C) 7.9 and (D) 8.05.